

Triplet spin resonance of the Haldane compound with interchain coupling

A. I. Smirnov,¹ V. N. Glazkov,¹ T. Kashiwagi,² S. Kimura,²
M. Hagiwara,² K. Kindo,³ A. Ya. Shapiro,⁴ and L. N. Demianets⁴

¹*P. L. Kapitza Institute for Physical Problems RAS, 119334 Moscow, Russia*

²*Center for Quantum Science and Technology under Extreme Conditions (KYOKUGEN),
Osaka University, 1-3 Machikaneyama, Toyonaka, Osaka 560-8531, Japan*

³*Institute for Solid State Physics (ISSP), University of Tokyo,
5-1-5 Kashiwanoha, Kashiwa, Chiba 277-8581, Japan*

⁴*A. V. Shubnikov Institute for Crystallography RAS, 117333 Moscow, Russia*

(Dated: October 25, 2018)

Spin resonance absorption of the triplet excitations is studied experimentally in the Haldane magnet $\text{PbNi}_2\text{V}_2\text{O}_8$. The spectrum has features of spin $S = 1$ resonance in a crystal field, with all three components, corresponding to transitions $|\pm 1\rangle \leftrightarrow |0\rangle$ and $|-1\rangle \leftrightarrow |1\rangle$, being observable. The resonance field is temperature dependent, indicating the renormalization of excitation spectrum in interaction between the triplets. Magnetic resonance frequencies and critical fields of the magnetization curve are consistent with a boson version of the macroscopic field theory,^{6,10} implying the field induced ordering at the critical field, while contradict the previously used approach of noninteracting spin chains.

PACS numbers: 75.50.Ee, 76.60-k.

I. INTRODUCTION

The inorganic dielectric $\text{PbNi}_2\text{V}_2\text{O}_8$, with the magnetic structure formed by chains of Ni^{2+} ($S=1$) ions, exhibits a Haldane like ground state.^{1,2} Due to anisotropy and interchain exchange the Haldane energy gap is reduced and $\text{PbNi}_2\text{V}_2\text{O}_8$ is close to the critical point of the quantum phase transition from a spin-liquid to an ordered easy-axis antiferromagnet.³ Besides, the spin-liquid phase may become unstable at the critical magnetic field, corresponding to the vanishing of the energy gap of triplet excitations. In Heisenberg exchange approximation the critical field value H_c and the energy gap Δ are related by a simple relation $g\mu_B\mu_0 H_c = \Delta$. The influence of the single-ion anisotropy on the Haldane spin chains was analysed theoretically by the exact diagonalization for finite chains,⁴ by a perturbative approach,^{4,5} as well as by macroscopic field theory methods.⁶ In the magnetic field range far below H_c all models result in the same energy levels, parametrized by the main gap, one or two anisotropy constants and g -factor. The perturbative description of excitations in the Haldane chain appears to be identical to the description of an isolated spin $S = 1$ in a crystal field.⁷ Extrapolated to the field of spin-gap closing, the perturbative approach yields critical fields

$$g\mu_B\mu_0 H_{\alpha c} = \sqrt{\Delta_\beta \Delta_\gamma}, \quad (1)$$

here the magnetic field is applied along principal direction α , while β and γ note other principal directions. For the uniaxial case the $S_z = \pm 1$ triplet components with the momentum of π have equal gaps $\Delta_x = \Delta_y$, and the gap of $S_z = 0$ component, Δ_z , is higher or lower depending on the anisotropy type. The value of the gap splitting caused by the crystal field is, in terms of $S = 1$ problem, the effective anisotropy constant $D_{eff} = \Delta_x - \Delta_z$. For Haldane chains $D_{eff} = -1.98D$ and $(2\Delta_x + \Delta_z)/3 = \Delta$,

where D is a single ion anisotropy constant contributing to the single ion Hamiltonian with the term DS_z^2 .

The spectrum of a real spin-gap system may be more complicated, as, e.g., for the Haldane magnet $\text{Ni}(\text{C}_2\text{H}_8\text{N}_2)_2\text{NO}_2(\text{ClO}_4)$ (abbreviated as NENP), when the spin gap remains non-zero due to the staggered g -tensor,⁸ or for the dimer spin-gap system TlCuCl_3 ,^{9,10} with a nonlinear frequency-field dependence near the critical field, at which the field-induced 3D ordering occurs, *etc.* $\text{PbNi}_2\text{V}_2\text{O}_8$ is a convenient model system for study the influence of 3D correlations and anisotropy on the spin-gap in a magnetic field, because this compound demonstrates a spin-gap split by the anisotropy, spin-liquid behavior below the critical field and field-induced 3D antiferromagnetic ordering above H_c .¹¹

The perturbative approach of noninteracting Haldane chains (in particular, formula (1)) was used¹² for $\text{PbNi}_2\text{V}_2\text{O}_8$ to derive the energy gaps from the critical field values. Further, the velocity of spin excitations, intrachain and interchain exchange integrals were found by fitting the inelastic neutron scattering intensity from a powder sample keeping the above spin gap values fixed.^{1,2,12} Nevertheless, the extrapolation of the perturbative approach to high fields may be doubtful. While it is justified by the exact diagonalization of the finite chain problem,⁴ the field-theory treatment⁶ has resulted in two models, diverging in high fields. The boson model should be exact in presence of interchain coupling of nearly a critical value, while fermion model is exact for a hypothetical Hamiltonian. Analogous theory considering a general case of a spin-gap magnet with the field-induced 3D ordering was developed in Ref.10. The source Lagrangian and relations between the critical fields in the bosonic model⁶ and in the macroscopic theory¹⁰ are identical. The results of the fermionic model are close to the perturbative theory and exact diagonalization of finite

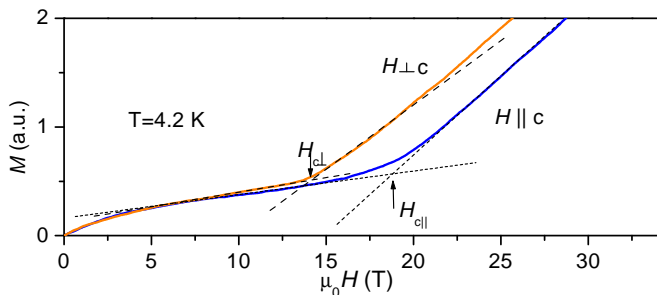


FIG. 1: Pulse field magnetization of the aligned sample of $\text{PbNi}_2\text{V}_2\text{O}_8$. Solid curves: experiment, dashed stright lines - extrapolations to $H_{c\perp,\parallel}$

chain problem, while the boson model and the model¹⁰ diverge from the perturbative curves near the critical field. Probably, this divergency should be ascribed to fluctuations, which are suggested to be suppressed (e.g. by 3D coupling) in the boson model of Ref. 6 and in the macroscopic theory of Ref. 10.

In the present paper we study the triplet excitations by means of the high-frequency electron spin resonance (ESR) spectroscopy which enables one to measure directly the frequencies of the transitions between the spin sublevels of the collective triplet states. We recover the splitting of the zero-field energy gap from the experiment and relate it to the difference between the critical fields H_{xc} and H_{zc} . The zero-field splitting of the triplet levels appears to be about one-half of the value estimated by the perturbative relation(1). At the same time, the spectrum of triplet excitations is well described by macroscopic models, implying 3D ordering at the critical field.^{6,10} Thus, the influence of the interchain coupling was found to be of importance for the magnetic excitation spectrum in the vicinity of the critical field.

II. EXPERIMENT

We used ceramic samples of $\text{PbNi}_2\text{V}_2\text{O}_8$ prepared as described in Ref.13 and magnetic field aligned samples prepared following Ref. 1 with the orientation of c -axis of crystallites parallel to the aligning field. Magnetization curves taken by the pulse technique are shown in Fig. 1. The critical field values derived from these curves are $\mu_0 H_{c\parallel} = 19 \pm 0.5$ T and $\mu_0 H_{c\perp} = 14 \pm 0.5$ T, which are well consistent with the data of Refs.1 and 11. The ESR spectra were measured both for ceramic and aligned samples, as microwave transmission *vs* magnetic field dependences. Magnetic field was created by a 16 T cryomagnet. Microwave signal in the frequency range 70-500 GHz was generated and detected by means of the vector network analyzer from the ABmm system at the KYOKUGEN Center.

A typical ESR spectrum of a ceramic sample and its evolution with temperature is presented for the frequency $f = 150$ GHz on Fig. 2. Analogous spectra for the

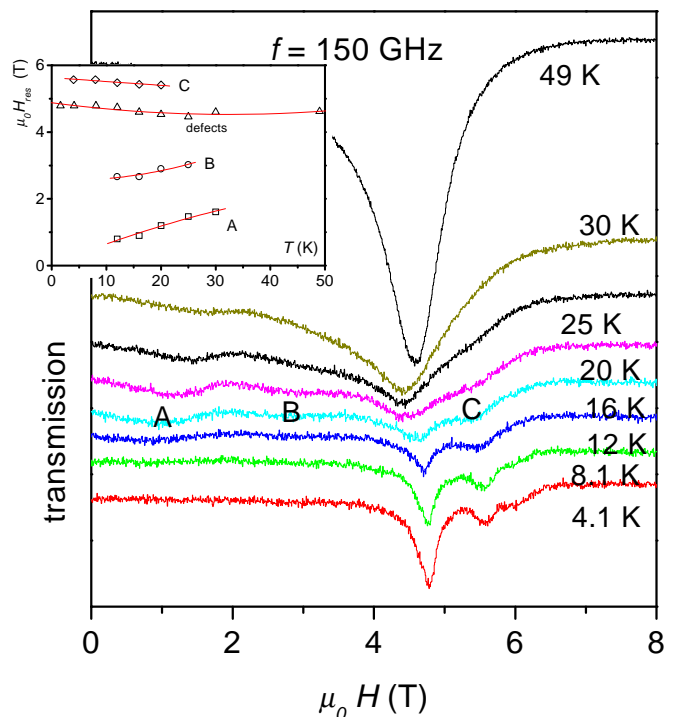


FIG. 2: 150 GHz ESR spectra of a $\text{PbNi}_2\text{V}_2\text{O}_8$ ceramic sample measured at different temperatures. Inset: Temperature dependence of the ESR fields A, B, C. Lines are guide to the eye.

aligned sample and the frequency of 275 GHz are presented on Fig. 3. At the temperatures above 30 K there is a single ESR line, corresponding to a typical exchange-narrowed Ni^{2+} ESR signal with g -factor value of 2.23. At cooling the sample we observe the diminishing of the intensity of this signal and appearing of three ESR lines apart from the high temperature ESR field. These signals are marked by letters A, B and C on Figs. 2 and 3. They disappear again at low temperatures, demonstrating a temperature dependent shift of the resonance field, as shown on the Insets of Figures. At low temperatures an upturn of the resonance absorption in g -factor range 1.9-2.2 with the maximum at $g = 2.2$ occurs. This low-temperature signal is due to defects and impurities. The intensity of marked signals, increasing with temperature, indicates a thermally activated nature of this kind of resonance. The separated lines of thermally activated absorption are distinctly seen in the temperature range 15-20 K, at lower temperatures the intensity is weak because of the spin gap, and at higher temperatures the lines merge into a single line. No absorption signal corresponding to the singlet-triplet transitions is observed.

Comparison of the ESR absorption of the ceramic and aligned samples at close frequencies is given on Fig. 4. Dashed arrows near the curve, corresponding to the ceramic sample, mark boundaries of the absorption band and letters A, B, C denote thermally activated lines for both samples. The central peak is ascribed to defects

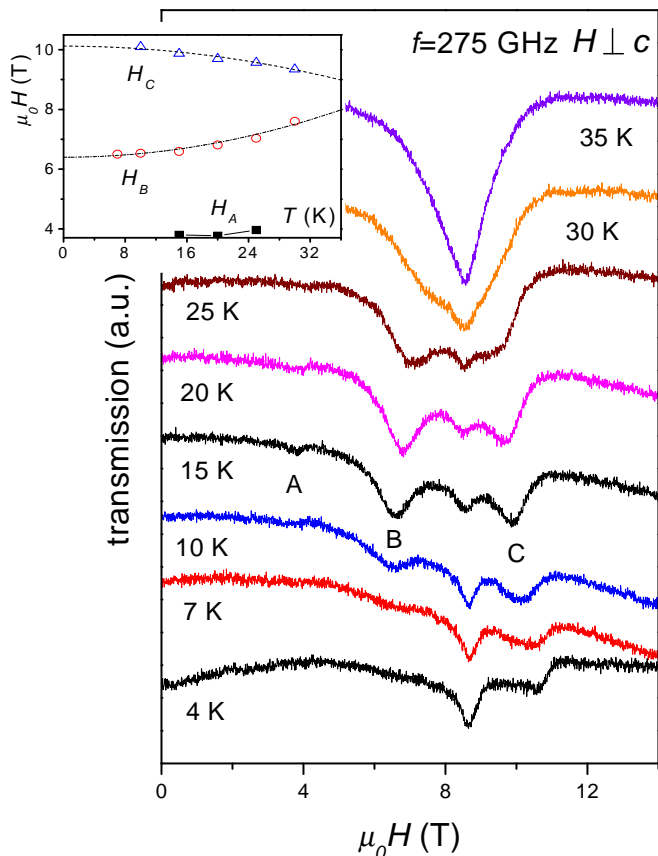


FIG. 3: 275 GHz ESR spectra of a $\text{PbNi}_2\text{V}_2\text{O}_8$ aligned sample measured at different temperatures for H perpendicular to the alignment axis. Inset: Temperature dependence of the ESR fields A, B, C. Lines are guide to the eye.

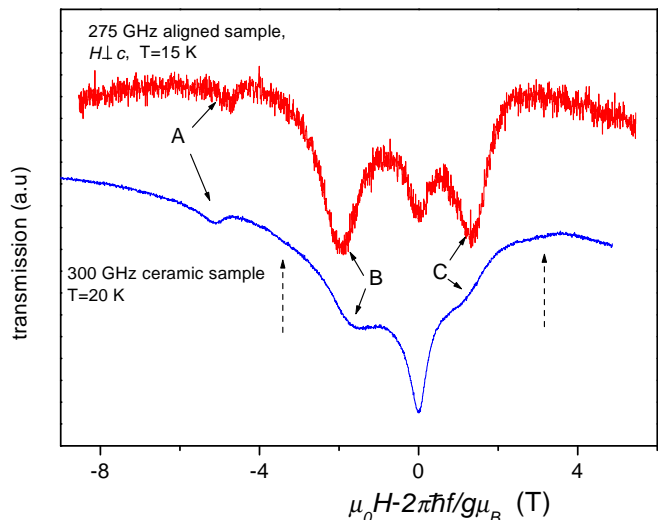


FIG. 4: 300 GHz ESR spectrum of a $\text{PbNi}_2\text{V}_2\text{O}_8$ ceramic sample at $T = 20$ K (lower curve) and 275 GHz spectrum of an aligned sample (upper curve).

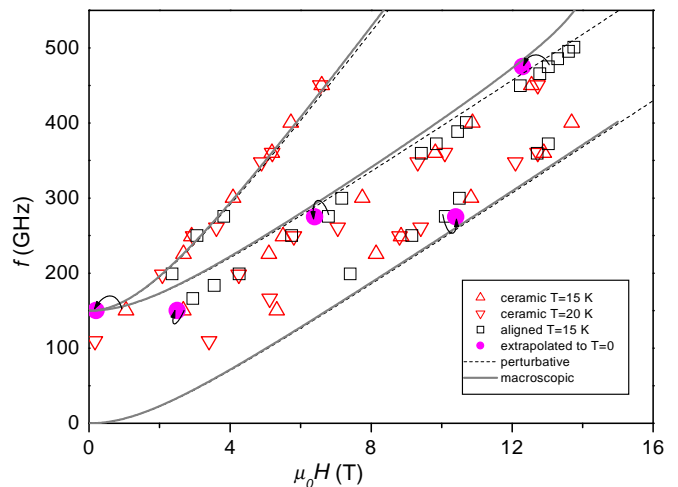


FIG. 5: Frequency-field diagram of the thermally activated magnetic resonance of $\text{PbNi}_2\text{V}_2\text{O}_8$ ceramic and aligned samples. Triangles and squares present experimental data for resonances marked by A, B, C. Lines are model calculations. Solid circles represent the extrapolations to $T=0$ noted by curved arrows.

and diminishes with temperature as a conventional paramagnetic resonance line. The analogous record of the aligned sample at $H \perp c$ has more distinct resonance lines at the positions B and C, than the ceramic sample. The positions of the local maxima of thermally activated absorption, taken at different frequencies, are plotted on Fig. 5.

III. DISCUSSION

A. General aspects

The lineshape of the thermally activated absorption (Figs. 2 and 4) corresponds approximately to the known ESR spectrum of a powder and crystal samples with $S = 1$ ions in an axial crystal field (see, e.g., Ref. 7). For a uniaxial crystal, this ESR spectrum, in case of $g\mu_B\mu_0 H \gg D$, consists of three resonance lines corresponding to the transitions $|\pm 1\rangle \leftrightarrow |0\rangle$ with $\Delta S_z = \pm 1$ and $|-1\rangle \leftrightarrow |1\rangle$ with $\Delta S_z = \pm 2$. Two resonance lines, corresponding to $\Delta S_z = \pm 1$, have larger intensity and are on both sides from the free spins resonance field $\mu_0 H_0 = 2\pi\hbar f / (g\mu_B)$. The distance between these two lines is $2D/g\mu_B$ for $H \parallel c$ and approximately $D/g\mu_B$ for $H \perp c$. Here D is a single ion anisotropy constant contributing to the single ion Hamiltonian with the term $D\hat{S}_z^2$. Naturally, for a powder sample there should be a band of absorption instead of resonance lines, the whole band width is $2D/g\mu_B$, and the maxima of absorption are near the resonance field of crystallites with $c \perp H$ because of their largest statistical weight (the field interval between maxima is again $D/g\mu_B$). In case of the easy plane anisotropy the intensity of the lower field maximum

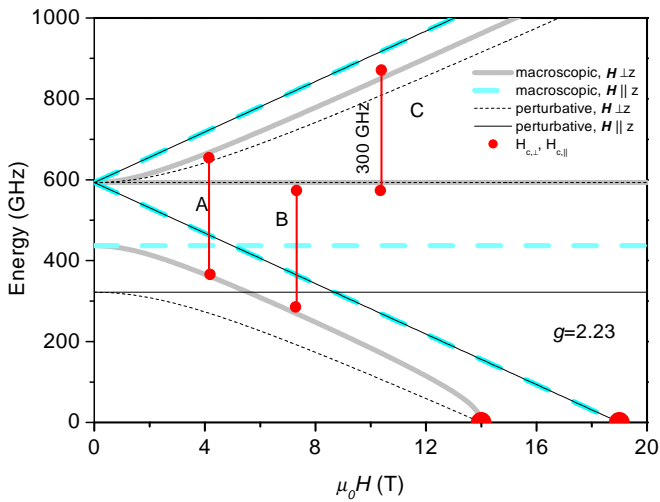


FIG. 6: Triplet energy levels in a spin gap magnet with $\mu_0 H_{c\perp}=14.0$ T and $\mu_0 H_{c\parallel}=19.0$ T, calculated for noninteracting Haldane chains⁴ (thin lines) and derived in the macroscopic model¹⁰ (thick lines). Vertical segments present observed transitions at $f=300$ GHz

is larger than that at the upper one because of a higher population of the lower spin sublevels. For the case of the easy axis anisotropy the relation between the intensities should be inverted.

Applying the above consideration of $S = 1$ magnetic ion in a crystal field we conclude, that the effective anisotropy of the triplet excitations is of the easy plane type ($D_{eff} > 0$). According to Ref. 4, D_{eff} and D are of different signes, thus, the single-ion constant D should be negative, which agrees with the easy axis anisotropy of the impurity induced ordered phase.¹³

Maximums of the absorption are separated by approximately 3.5 T, which corresponds to $D_{eff} \simeq 110$ GHz (here and farther on we assume $g = 2.23$, as proved by ESR at $T > 30$ K). The leftmost absorption line demonstrates a characteristic frequency-field dependence (Fig. 5) with asymptote $f = 2g\mu_B\mu_0 H/(2\pi\hbar)$, marking a two-quantum transition with $\Delta S_z = \pm 2$. Its zero-field gap is equal to the splitting of the triplet sublevels⁷. Observation of this absorption at the frequency 150 GHz indicates directly, that the splitting of the triplet levels by the effective crystal field is less than or about 150GHz.

The perturbative approach⁴ yields by (1) the zero-field gaps $E_{min1} = 320 \pm 10$ GHz and $E_{min2} = 590 \pm 10$ GHz. The corresponding splitting of 270 GHz is twice as large as estimated from the observed ESR lines. Alternatively, energy levels of the triplet excitations can be calculated within the boson model,^{6,10} which imply 3D ordering above the critical field. Details of the calculation are given in Appendix. For $D_{eff} > 0$ the gaps are related to the critical fields as follows:

$$g\mu_B\mu_0 H_{c\perp} = E_{min1}, \quad g\mu_B\mu_0 H_{c\parallel} = E_{min2} \quad (2)$$

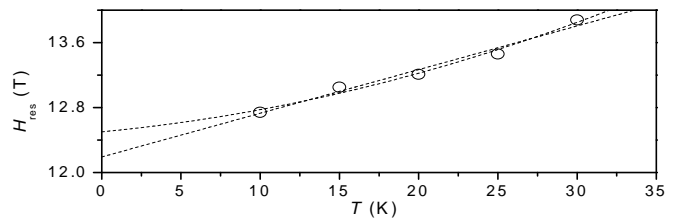


FIG. 7: Temperature dependence of the resonance field of the mode B at the frequency 475 GHz for the aligned sample at $\mathbf{H} \perp c$. Dashed lines are linear and second order polynom extrapolations to zero temperature.

From the critical field values we get here $E_{min1} = 440 \pm 10$ GHz and $E_{min2} = 590 \pm 10$ GHz. The corresponding splitting of 150 GHz is in much better agreement with the above experimental results. The calculated triplet sublevels for perturbative and macroscopic models are presented at the Fig.6. Here all theories are locked to the observed values of critical fields. The difference in E_{min1} occurs due to the nonlinear field dependence of the energy of the lowest triplet sublevel near $H_{c\perp}$ in the macroscopic models. It should be noted, that in low fields, i.e. far from the critical point, all models would demonstrate identical results when they would be locked on the same energy gaps at $H = 0$.

The frequency-field dependence for the case $\mathbf{H} \perp c$ calculated in a perturbative approach and in the macroscopic models is presented in Fig. 5. It should be noted that no fitting parameters are used here, the value of zero field splitting, $D_{eff} = E_{min2} - E_{min1}$ is taken from critical fields using relations (2). The resonance fields were taken at $T = 15$ and 20 K, while critical fields are measured at 4.2 K. Thus, we have to extrapolate the observed resonance fields to zero temperature. The temperature evolution of the ESR spectra, analogous to that shown in Fig. 3, was followed for the frequencies 150, 275 and 475 GHz. The resonance fields, extrapolated to $T=0$ are shown on Fig.5 by solid circles, pointed by curved arrows. The data, extrapolated to zero temperature, lie on the model curve within the experimental error.

Note that the energy levels predicted in Refs. 1, 2 and 12 by use of the perturbative model⁴ ($D_{eff} = 270$ GHz and $E_{min2}/(2\pi\hbar) = 590$ GHz) does not correspond to any extent. Thus, the experimental ESR frequencies are in a agreement with the energy levels predicted by the macroscopic theories,^{6,10} rather than with the theory considering isolated Haldane chains.⁴

B. Modeling

We performed a model calculation of the ESR absorption for the powder sample of a spin gap magnet with gapped triplet excitations (see Figs. 9 and 8). The modeling was performed by two methods, giving practically

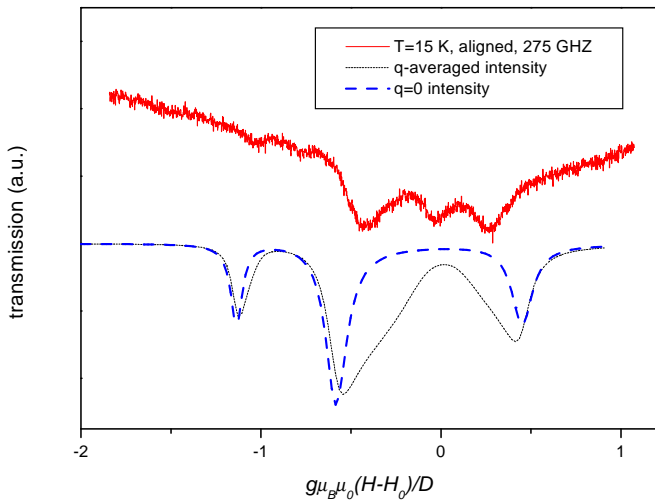


FIG. 8: 275 GHz ESR spectrum of a $\text{PbNi}_2\text{V}_2\text{O}_8$ aligned sample at $T=15$ K, $\mathbf{H} \perp c$, and the calculated spectrum in $S=1$ model for the triplets at the bottom of the excitations zone ($q=0$) and a spectrum, averaged over the excitations, excited at $T=20$ K. Parameters used are: $E_{min2}=590$ GHz, $D_{eff}(0)=150$ GHz, ESR linewidth 10 GHz, $s=4895$ GHz, $g=2.23$

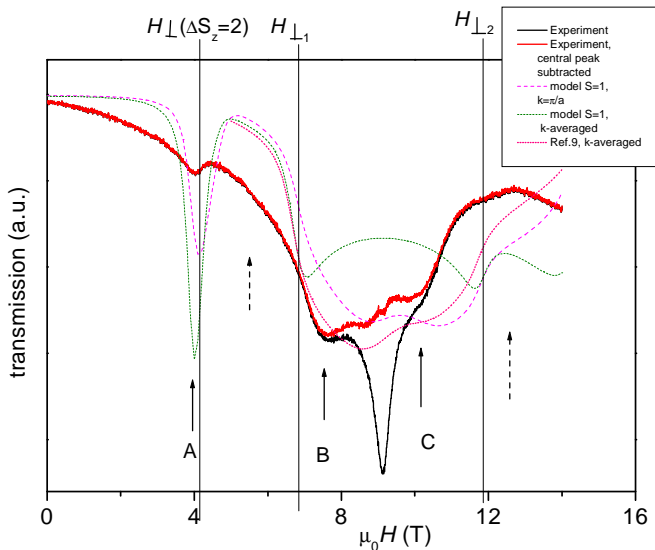


FIG. 9: 300 GHz ESR spectrum of a $\text{PbNi}_2\text{V}_2\text{O}_8$ ceramic sample at $T=20$ K (black solid line), the same spectrum with the defects Lorentzian line subtracted and model spectra as described in the text. Vertical lines are at the resonance fields for crystallites with the field lying in the basal plane. Parameters used are: $E_{min2}=590$ GHz, $D_{eff}(0)=150$ GHz, ESR linewidth 10 GHz, $s=4895$ GHz, $g=2.23$

similar results for the lineshape and positions of the maxima of ESR absorption.

For the first method we considered the energy levels of effective spin $S=1$ ascribed to a triplet excitation mode with a wavevector \mathbf{k} . The population numbers for the $S_z = \pm 1$ and $S_z = 0$ spin sublevels of a triplet excitation

mode were calculated according to the Plank's distribution function. The effective anisotropy constant, equal to the zero field splitting of a triplet sublevels is defined as

$$D_{eff}(\mathbf{k}) = \hbar(\omega_x(0, \mathbf{k}) - \omega_z(0, \mathbf{k})) \quad (3)$$

here $\omega_{x,y}(0, \mathbf{k})$ and $\omega_z(0, \mathbf{k})$ are zero-field cyclic frequencies of the triplet excitations carrying effective spin projection S_z^{eff} equal to ± 1 or zero correspondingly. We calculated the microwave absorption for effective spins $S=1$ in a uniaxial crystal field according the standard ESR procedure, i.e. calculating transition frequencies, matrix elements of the transitions and difference of the population numbers⁷. The spectrum of the triplet excitations in zero field is taken in the form^{6,10,12}:

$$\omega_{x,y}(\mathbf{q}) = \sqrt{\omega_{x,y}^2(0) + s^2 q^2} \quad (4)$$

$$\omega_z(\mathbf{q}) = \sqrt{\omega_z^2(0) + s^2 q^2} \quad (5)$$

with $q = \pi - ka$, $s=4895$ GHz (Ref.2), and $\omega_z(0)/(2\pi) = 440$ GHz, $\omega_{x,y}(0)/(2\pi) = 590$ GHz derived from the fields $H_{c\parallel}$ and $H_{c\perp}$ according to Ref. 10 as shown on Fig. 6. The field dependences of $\hbar\omega_\alpha(k)$ are derived as the energies of corresponding sublevels of an effective spin $S=1$ in a crystal field with the anisotropy constant $D_{eff}(k)$.

This modeling also provides the low-field $\Delta S = \pm 2$ transition, which is allowed in the canted orientations of the magnetic field with respect to anisotropy axis.

For the second method we used the excitations frequencies, given by the macroscopic models.^{6,10} These frequencies can be calculated for an arbitrary \mathbf{H} and \mathbf{q} (see Appendix) in the low frequency approximation $\hbar\omega_\alpha \ll J$. Since this model does not provide information on matrix elements of the transitions, which are necessary to calculate intensity of the corresponding ESR absorption, we have used this model only at high fields taking the matrix elements for $\Delta S_z = \pm 1$ transitions to be equal and field independent. Population numbers of the excited states were taken according to the Plank's distribution function again.

The model microwave absorption due to the excitations with the energy at the bottom of the zone ($q=0$) is shown in Fig. 8 along with the model absorption curve at $T=15$ K, when the excitations away of the zone bottom are also excited. Despite of the smaller value of D_{eff} of the high energy excitations, the peaks of absorption remain at the same positions due to a large spectral density at the zone bottom. At heating, the absorption curve becomes asymmetric with enlarging of the intensity in the field range, corresponding to resonance for smaller D_{eff} , as predicted in Ref. 6. For modeling of the ESR absorption of the ceramic samples, we made the averaging over the random orientations of crystallites and, again, over the one-dimensional \mathbf{k} -space. The calculated

lineshape, presented by the dashed curve on Fig. 9 corresponds qualitatively to the observed line, if we subtract the central peak of absorption, produced by the defects, as shown on the Fig. It should be noted that the singularity in the form of the step of absorption is close to the maximum of absorption for the single- \mathbf{k} calculation, both singularities are due to the maximum of the statistic weight of the crystallites with the four fold axis perpendicular to the magnetic field. For the \mathbf{k} -space integrated absorption the steps are at the same positions, while the maxima are smeared due to the contribution of the higher energy excitations which have smaller value of $D_{eff}(\mathbf{k})$. The results of the modeling are practically independent on the natural ESR linewidth changing in the range 1–10 GHz.

C. Temperature dependent ESR

The temperature dependence of the triplet ESR field observed in the present work may be, probably, attributed to an interaction between the triplets, analogous to the spin-wave frequencies in conventional ferromagnetic and antiferromagnets, which is known to be renormalized with excitation of magnons (see, e.g., Refs. 16 and 17). The temperature dependence of the triplet excitation spectrum was observed also for the dimer spin-gap compound TlCuCl_3 .¹⁵ An alternative reason for the temperature dependence of D_{eff} and the triplet excitation spectrum may be the change of the correlation length with heating. However, according to experiments¹⁴, the correlation length is reduced only for 20 % at the temperature of a half of the intrinsic Haldane gap $0.41J$, as in our case. Apparently, this may not substantially change the effective anisotropy constant of triplet excitations. The excitation of the triplets apart from the bottom of the excitation spectrum also may not change the position of the absorption maxima, despite they should have smaller D_{eff} . As noted in Ref. 6, the influence of higher energy excitations will result in an asymmetric form of the ESR lines but not in the shift of the absorption maximum.

IV. CONCLUSIONS

In conclusion, the ESR spectrum of triplet excitations in a Haldane magnet $\text{PbNi}_2\text{V}_2\text{O}_8$ demonstrates a temperature dependence, probably, due to the interaction between the excitations. ESR of triplet excitations is satisfactorily modeled without fitting parameters, using the experimental values of critical fields. The relation between the critical fields and energy gaps corresponds to the boson model of Ref. 6 and macroscopic theory¹⁰ and contradicts the fermion model of Ref. 6 and isolated chain calculations of Ref. 4. This indicates, supposedly, a strong influence of the 3D correlations on the spectrum of excitations in $\text{PbNi}_2\text{V}_2\text{O}_8$.

Acknowledgments

Authors are indebted to A. M. Farutin, V. I. Marchenko, T. Sakai and M. E. Zhitomirsky for discussions. This work was in part supported by the Grant-in-Aid for Scientific Research on Priority Areas from the Japanese Ministry of Education, Culture, Sports, Science and Technology and by the Russian Foundation for Basic Research grant 06-02-16509. Some of these studies were done under a Foreign Visiting Professor Program in KYOKUGEN, Osaka University.

V. APPENDIX

Following Ref.10, the Lagrangian for the vector field $\boldsymbol{\eta}$ corresponding to $S = 1$ excitation for the crystal with the uniaxial symmetry is

$$L = \frac{1}{2}(\dot{\boldsymbol{\eta}} + \gamma[\boldsymbol{\eta}\mathbf{H}])^2 - \frac{A}{2}\boldsymbol{\eta}^2 - \frac{G_{ij}}{2}\partial_i\boldsymbol{\eta}\partial_j\boldsymbol{\eta} + \frac{b}{2}(\eta_x^2 + \eta_y^2 - 2\eta_x^2), \quad (6)$$

here $\gamma = g\mu_B\mu_0/\hbar$.

Corresponding equation of motion has the form

$$\ddot{\boldsymbol{\eta}} + 2\gamma[\dot{\boldsymbol{\eta}}\mathbf{H}] - \gamma^2 H^2 \boldsymbol{\eta} + \gamma^2 \mathbf{H}(\boldsymbol{\eta}\mathbf{H}) + A\boldsymbol{\eta} - G_{ij}\partial_i\partial_j\boldsymbol{\eta} - b \begin{pmatrix} \eta_x \\ \eta_y \\ -2\eta_z \end{pmatrix} = 0. \quad (7)$$

The frequencies at $k = \pi/a$ and $H = 0$ are

$$\omega_{x,y}^{(0)} = \sqrt{A_{xx}} = \sqrt{A-b} \quad (8)$$

$$\omega_z^{(0)} = \sqrt{A_{zz}} = \sqrt{A+2b} \quad (9)$$

The field and k -dependences for principal directions of the magnetic field are:

for $\mathbf{H} \parallel z$:

$$\omega_{x,y} = \sqrt{A_{xx} + s^2 q^2} \pm \gamma H \quad (10)$$

$$\omega_0 = \sqrt{A_{zz} + s^2 q^2} \quad (11)$$

for $\mathbf{H} \parallel x$:

$$\omega_{x,y}^2 = \gamma^2 H^2 + \frac{A_{xx} + A_{zz}}{2} + s^2 q^2 \pm \left[\frac{(A_{xx} - A_{zz})^2}{4} + 2\gamma^2 H^2 (A_{xx} + A_{zz}) + 4\gamma^2 H^2 s^2 q^2 \right]^{1/2} \quad (12)$$

$$\omega_0 = \sqrt{A_{zz} + s^2 q^2} \quad (13)$$

here $q = k - \pi/a$.

For an arbitrary orientation the frequencies may be found by solving the secular equation

$$x^3 + (2h^2 + A_{zz} - A_{xx})x^2 - h^2(4(A_{xx} + q^2s^2) - h^2 + (A_{zz} - A_{xx})(1 - 3\cos^2\theta))x - (A_{zz} - A_{xx})h^2\cos^2\theta(4(A_{xx} + q^2s^2) - h^2) = 0 \quad (14)$$

here $h = \gamma H$, $x = -\omega^2 + q^2s^2 + A_{xx}$, θ is the angle between the magnetic field and z -axis.

Critical field in the arbitrary orientation of the applied field for the effective easy-plane anisotropy of triplet excitations ($b < 0$) is given by the equation

$$\gamma H_c(\theta) = \frac{\omega_z^{(0)}\omega_{x,y}^{(0)}}{\sqrt{(\omega_{x,y}^{(0)})^2 + \left((\omega_z^{(0)})^2 - (\omega_{x,y}^{(0)})^2\right)\cos^2\theta}} \quad (15)$$

while for the effective easy-axis anisotropy of triplet excitations ($b > 0$) H_c is orientation independent

$$\gamma H_c = \frac{\hbar}{g\mu_B}\omega_{x,y}^{(0)} \quad (16)$$

¹ Y. Uchiyama *et al.*, Phys. Rev. Lett. **83**, 632 (1999).

² A. Zheludev *et al.*, Phys. Rev. B **62**, 8921 (2000).

³ T. Sakai and M. Takahashi, Phys. Rev. B **42**, 4537 (1990).

⁴ O. Golinelli *et al.*, J. Phys. Condens. Matter **5**, 7847 (1993).

⁵ L.-P. Regnault, I. A. Zaliznyak, and S. V. Meshkov, J. Phys.: Condens. Matter **5**, L677 (1993).

⁶ I. Affleck, Phys. Rev. B **46**, 9002 (1992).

⁷ A. Abragam and B. Bleaney, Electron Paramagnetic Resonance of Transition Ions (Clarendon, Oxford, 1970).

⁸ M. Sieling *et al.*, Phys. Rev. B **61**, 88 (2000).

⁹ A. Kolezhuk *et al.*, Phys. Rev. B **70**, 020403 (2004).

¹⁰ A.M. Farutin, V. I. Marchenko JETP **131** 860 (2007).

¹¹ N. Tsujii *et al.*, Phys. Rev. B **72**, 104402 (2005).

¹² A. Zheludev *et al.*, Phys. Rev. B **64**, 134415 (2001).

¹³ A.I. Smirnov *et al.*, Phys. Rev. B **65**, 174422 (2002).

¹⁴ F. Tedoldi *et al.*, Phys. Rev. Lett. **83**, 412 (1999).

¹⁵ V.N.Glazkov *et al.*, Phys. Rev. B **69**, 184410 (2004).

¹⁶ F. Dyson, Phys Rev **102**, 1217, 1230 (1956).

¹⁷ L. A. Prozorova, A.I.Smirnov, Zh. Eksp. Teor. Fiz. **74** 1554 (1978) [Sov. Phys. JETP **47** 812 (1978)]